A fully nonlinear characteristic method for gyrokinetic simulation

S. E. Parker and W. W. Lee

Citation: Physics of Fluids B: Plasma Physics **5**, 77 (1993); doi: 10.1063/1.860870
View online: http://dx.doi.org/10.1063/1.860870
View Table of Contents: http://aip.scitation.org/toc/pfb/5/1
Published by the American Institute of Physics

A fully nonlinear characteristic method for gyrokinetic simulation

S. E. Parker and W. W. Lee
Princeton Plasma Physics Laboratory, Princeton University, Princeton, New Jersey 08543

(Received 17 June 1992; accepted 16 September 1992)

A new scheme that evolves the perturbed part of the distribution function along a set of characteristics that solves the fully nonlinear gyrokinetic equations is presented. This low-noise nonlinear characteristic method for particle simulation is an extension of the partially linear weighting scheme, and may be considered an improvement over existing δf methods. Some of the features of this new method include the ability to keep all nonlinearities, particularly those associated with the velocity space, the use of conventional particle loading techniques, and also the retention of the conservation properties of the original gyrokinetic system in the numerically converged limit. The new method is used to study a one-dimensional drift wave model that isolates the parallel velocity nonlinearity. A mode coupling calculation for the saturation amplitude is given, which is in good agreement with the simulation results. Finally, the method is extended to the electromagnetic gyrokinetic equations in general geometry.

I. INTRODUCTION

An outstanding issue in gyrokinetic simulation (and in particle-in-cell simulation in general) is that often it is necessary to use a rather large number of particles to resolve the physics of interest. The concern being that thermal fluctuations (or noise) and lack of sampling (or resolution) of the two- to six-dimensional phase space caused by a finite number of particles may obscure the physical process being modeled. For example, the broadband density fluctuations existing in tokamak plasmas usually have an average level of a fraction of 1% or less. Thus modeling such plasmas requires a very large number of particles for proper resolution, such that $N_{\rm tot} \gg 1/(\delta n/n)^2 \approx 10^6$.[1] Early on, it was recognized by Beyers and others that improvements in noise properties could be made by "quiet starts,"[2,3] and also by linearization techniques that track the perturbed quantities in terms of the equilibrium trajectories.[2,4,5] More recently, Dimits and Lee[6] developed a linear and a "partially linear" low-noise scheme by allowing the particle weights to evolve in time. In the linear scheme the particle weights follow the equilibrium trajectories. In the partially linearized scheme, the $E\times B$ nonlinearity is retained by adding this drift to the equilibrium (zeroth-order) orbit. There have been other investigations[7,8] of a class of techniques often called δf methods, but no schemes up to this point have reported results where the parallel velocity nonlinearity is retained. Therefore the correctness of these schemes has never been verified.

The nonlinear characteristic method presented here is similar in spirit to previous weighting schemes;[6] however, the fully nonlinear trajectories are evolved and a consistent evolution equation is used for the particle weights. We begin by presenting the new method for the electrostatic slab case and the associated conservation properties of particle number, momentum, and total energy. We then present gyrokinetic simulations of a simple one-dimensional drift wave instability in a shearless slab. This model isolates $E_\parallel \partial_{v_\parallel} \delta f$ nonlinearity and allows us to study the associated nonlinear physics. A three-wave mode coupling theory that gives a saturation level of $e|\phi|/T_e \approx 5.5\gamma^2/(k_\parallel v_{te})^2$ is presented and is much lower than the calculation of Sagdeev and Galeev,[9] $e|\phi|/T_e \approx \frac{1}{4}(k_\perp \rho_s)^2$. There is excellent agreement between the theory and the simulation in terms of linear frequency and growth rate. The amplitude for nonlinear saturation also agrees with our theoretical prediction. The conservation properties of the simulation plasma have also been investigated. It is found that the conservation of number density, momentum, and energy in the nonlinear stages of the simulation can be achieved only if we use a sufficiently large number of particles, small time steps, and a small grid cell size. Finally, we discuss the application of the nonlinear characteristic method to the general electromagnetic (nonuniform equilibrium magnetic field) gyrokinetic equations.

II. NONLINEAR CHARACTERISTIC METHOD

As mentioned earlier, devising a scheme where only the perturbed part of the distribution function is evolved has been previously investigated.[6–8] It was recognized that, by evolving only the perturbed part of the distribution δf, one could remove the initial noise associated with the equilibrium f_0 due to the use of a finite number of particles.[2,4–6,8] The scheme we present here is similar to the previously proposed δf methods,[7,8] but we take into account the discrete representation of the characteristics as was done for the partially linearized scheme.[6]

Let us begin by writing the distribution function $f(\mathbf{R},v_\parallel,\mu,t)$ in the familiar way as $f=f_0+\delta f$, where $\mathbf{R}$ is the guiding-center coordinate, $v_\parallel$ is the velocity parallel to the magnetic field, $\mu \equiv v_\perp^2/(2\Omega)$ is the magnetic moment and is assumed constant ($\dot{\mu}=0$), $\Omega \equiv eB/(mc)$, f_0 is the equilibrium background distribution and is independent of time, and δf is the perturbed time-dependent part of the distribution. For $(k_\perp \rho_i)^2 \ll 1$, the gyrokinetic equation for δf in the electrostatic slab limit is[10,11]

 0899-8221/93/010077-10$06.00

$$\partial_t \delta f + \mathbf{v}_E \cdot \nabla \delta f + v_\parallel \nabla_\parallel \delta f + (q/m) E_\parallel \partial_{v_\parallel} \delta f$$

$$= -\mathbf{v}_E \cdot \nabla f_0 - (q/m) E_\parallel \partial_{v_\parallel} f_0 , \tag{1}$$

where $\rho_i \equiv v_{ti}/\Omega_i$ is the ion gyroradius, $\mathbf{v}_E \equiv c\mathbf{E}/B \times \hat{\mathbf{b}}$ is the $\mathbf{E}\times\mathbf{B}$ drift. The corresponding gyrokinetic Poisson equation in the small $(k_\perp \rho_i)^2$ limit is

$$(\rho_s/\lambda_D)^2 \nabla_\perp^2 \phi = -4\pi e(n_i - n_e), \tag{2}$$

where $\rho_s \equiv \sqrt{\tau}\rho_i$, $\tau \equiv T_e/T_i$, $\lambda_D \equiv \sqrt{T_e/(4\pi n_0 e^2)}$ is the Debye length, and

$$n = \int \delta f \, dv_\parallel \, d\mu. \tag{3}$$

The characteristics (or trajectories) of Eq. (1) are

$$\dot{v}_\parallel = (q/m) E_\parallel , \tag{4}$$

$$\dot{\mathbf{R}} = v_\parallel \hat{\mathbf{b}} + \mathbf{v}_E , \tag{5}$$

and along these characteristics δf is changing because the right-hand side of Eq. (1) is nonzero. The evolution equation for δf along the trajectories is

$$\dot{\delta f} = -\mathbf{v}_E \cdot \nabla f_0 - (q/m) E_\parallel \partial_{v_\parallel} f_0 . \tag{6}$$

Now, we simply need to solve Eqs. (4)–(6). At first glance, one might consider loading a large number of characteristics (or particles), each having its own δf, evolve the system in time, and then weight the δf's to the grid to obtain field quantities. However, one needs to examine carefully how δf is being numerically represented and whether Eq. (1) or (6) is indeed being solved correctly.

We begin by defining the "particle weight" as

$$w_i \equiv \left. \frac{\delta f}{g} \right|_{\mathbf{x}=\mathbf{x}_i, v_\parallel = v_{\parallel i}, \mu=\mu_i, t} , \tag{7}$$

where, as above, δf is the perturbed part of the physical distribution, and g is the numerically loaded and evolved particle distribution function. At this point, g does not necessarily equal the physical distribution function. In a fashion similar to the partially linear weighting scheme,[6] except now the fully nonlinear trajectories are evolved, δf in the simulation is represented as

$$\delta f(\mathbf{R}, v_\parallel, \mu, t) = \sum_{i=1}^{N} w_i S(\mathbf{R} - \mathbf{R}_i) \delta(v_\parallel - v_{\parallel i}) \delta(\mu - \mu_i), \tag{8}$$

where N is the total number of particles and S is the particle shape function. Equation (8) easily follows from the definition of the w_i in Eq. (7), using $g = \Sigma_{i=s}^{N} (\mathbf{R} - \mathbf{R}_i) \delta(v_\parallel - v_{\parallel i}) \delta(\mu - \mu_i)$, and assuming that all the grid quantities have a small spatial (or long wavelength) variation compared to the particle size, permitting the use of the following relation:

$$\sum_i u(\mathbf{R}_i) S(\mathbf{R} - \mathbf{R}_i) = \sum_i [u(\mathbf{R}) - (\mathbf{R} - \mathbf{R}_i) \cdot \nabla u(\mathbf{R}) + \cdots] S(\mathbf{R} - \mathbf{R}_i) \tag{9}$$

$$\approx u(\mathbf{R}) \sum_i S(\mathbf{R} - \mathbf{R}_i), \tag{10}$$

where u is an arbitrary spatial function. This is similar to assuming that the spatial shape of the particle is a δ function. In the simulation, each particle (or trajectory) is associated with a phase-space volume element. The shape of this element may contort, but the volume remains constant.

Next, by taking the total time derivative of Eq. (7), and using $\dot{g} = 0$ along with Eq. (6), we obtain

$$\dot{w}_i = -\left(\mathbf{v}_E \cdot \frac{\nabla f_0}{g} + \frac{q}{m} E_\parallel \frac{\partial_{v_\parallel} f_0}{g} \right)_{\mathbf{R}=\mathbf{R}_i, v_\parallel = v_{\parallel i}, \mu=\mu_i, t} . \tag{11}$$

One way to solve Eq. (11) is to note that the function g satisfies the full nonlinear gyrokinetic equation so that g is constant along a trajectory. One can then use the relation $g(\mathbf{R}_i, v_{\parallel i}, \mu_i, t) = g[\mathbf{R}_i(t=0), v_{\parallel i}(t=0), \mu_i, t=0]$. Since the initial loading is arbitrary, one can, for example, load a uniform distribution $g(t=0) = \text{const}$ independent of the phase-space variables, which seems to be the approach proposed by Kotschenruether.[8]

Typically, for low-frequency microinstabilities, the resonant velocities are smaller than the thermal velocity of the species. Thus, a nonuniform loading (e.g., the Maxwellian distribution) in velocity space is much more desirable than a uniform one because higher phase-space resolution (i.e., more particles) is present where the wave is in resonance with the distribution function ($\omega/k_\parallel = v_\parallel$). One problem associated with the nonuniform loading for the existing δf schemes[8] is that additional particle arrays (or calculations) are needed to keep track of $g_i(t=0)$. Moreover, numerical difficulties may arise from the denominators of Eq. (11) for particles with small values of $g_i(t=0)$, i.e., those initially located at the tail of the distribution. These are some potential drawbacks for using Eq. (11) to evaluate w_i along with $g_i = g_i(t=0)$.

We now present the nonlinear characteristic method, which avoids these problems. One loads the particles with the equilibrium distribution $g(t=0) = f_0$ (as above, g is the particle distribution) in the same manner as in a conventional particle simulation. Then, assuming proper numerical resolution, $g = f = f_0 + \delta f$ throughout the simulation. Using the relation $1/f = (1/f_0)(1 - \delta f/f)$, along with Eqs. (8) and (11), we arrive at

$$\dot{w}_i = -(1 - w_i) \left(\mathbf{v}_E \cdot \frac{\nabla f_0}{f_0} + \frac{q}{m} E_\parallel \frac{\partial_{v_\parallel} f_0}{f_0} \right)_{\mathbf{x}=\mathbf{x}_i, v_\parallel = v_{\parallel i}, \mu=\mu_i, t} . \tag{12}$$

Equation (12) along with Eqs. (4), (5), and (8) are the crux of the new nonlinear characteristic method. As usual,

one uses Eqs. (2) and (3) to complete the simulation time loop. The equilibrium gradients in Eq. (12) are evaluated using the smooth analytic expression for f_0. Besides the nonlinearities appearing as perturbations to the zeroth-order trajectories [$E_\parallel$ and $\mathbf{v}_E$ in Eqs. (4) and (5)], there is the additional factor $(1-w_i)$ in the evolution of the equation for the weights in Eq. (12). This factor, which is essential to the nonlinear physics and the conservation properties of the simulation plasma, describes the difference between f_0 and $f(t)$ in the source term, as indicated by Eq. (11). For an arbitrary loading where $g_i(t=0)\neq f_i(t=0)$, the factor $(1-w_i)$ on the right-hand side of Eq. (12) needs to be replaced by the factor $[f_i(t=0)/g_i(t=0)-w_i]$. In such a case, an additional particle array would be required to keep track of the constant $f_i(t=0)/g_i(t=0)$. For most applications, $\delta f(t=0)/f(t=0)$ is very small, so that $f_0\approx f(t=0)$, and distinguishing between the equilibrium f_0 and the initial condition $f(t=0)$ is not necessary.

Let us now discuss the conservation of the total particle number, momentum, and total energy associated with the new nonlinear weighting scheme. First, we examine the change in "the number of particles" by taking the zeroth velocity moment of Eq. (1). Using Eq. (8) and assuming that the sum of the w_i's is nearly zero initially, we then obtain

$$\sum_i w_i(t)=0. \tag{13}$$

The momentum conservation can be derived by taking the first velocity moment of Eq. (1),

$$\partial_t\left(\int v_\parallel\,\delta f\,d\mathbf{R}\,d\mu\,dv_\parallel\right)-\frac{q}{m}\left(\int nE_\parallel\,d\mathbf{R}\right)=0, \tag{14}$$

which, along with Eqs. (2) and (8), then gives

$$\sum_\alpha m_\alpha \sum_i v_{\parallel\,\alpha i}\,w_{\alpha i}=0, \tag{15}$$

where n is given by Eq. (3) and α denotes species. To calculate the change in energy,[1] we take the second velocity moment of Eq. (1) for both the ions and the electrons and use Eq. (2). Again, if we take the particle weights and field to be zero at $t=0$, then the simulation should maintain the following energy conservation:

$$\sum_\alpha \frac{m_\alpha}{2}\sum_i(\mu_{\alpha i}+v_{\parallel\,\alpha i}^2)w_{\alpha i}+\left(\frac{\rho_s}{\lambda_D}\right)^2\frac{1}{8\pi}\int|\nabla_\perp\phi|^2 d\mathbf{R}=0. \tag{16}$$

We expect Eqs. (13)–(16) to hold for a simulation plasma in the limit of a large number of particles and fine space and time resolution. In the next section, we will examine the validity of these conservation properties in a simulation using a finite number of particles. This important exercise serves as a verification of the formal correctness of the proposed scheme as well as a test of its practicality. Most of all, we will show that the scheme is a useful alternative to conventional particle methods.

III. ONE-DIMENSIONAL DRIFT WAVE SIMULATION

We now present simulation results using the new method checking linear and nonlinear physics as well as the conservation properties. For simplicity, a one-dimensional drift wave problem is chosen as an example. In this one-dimensional model, the $E\times B$ nonlinearity is not present, so the $E_\parallel\,\partial_{v_\parallel}\delta f$ nonlinearity is the only mechanism for saturation. This is the term that has been neglected in the previous scheme[6] on the assumption that, in the more realistic two- and three-dimensional geometries, it is the $E\times B$ nonlinearity that is the dominant saturation mechanism. However, this may not be true for the cases with elongated modes (e.g., $k_x\ll k_y$), which we will discuss later. Moreover, as suggested in Refs. 10 and 11, the $E_\parallel\,\partial_{v_\parallel}\delta f$ nonlinearity may be important for the steady-state transport for gradient-driven microinstabilities.

In this problem, the one spatial dimension y is perpendicular to the spatial gradients, which are in the x direction, and is almost perpendicular to the magnetic field, $\hat{\mathbf{b}}=\hat{\mathbf{z}}+\theta\hat{\mathbf{y}}$, $\theta\ll 1$. Here, both x and z are ignorable coordinates for the perturbation quantities. The one-dimensional version of Eq. (1) for both the ions and the electrons is

$$\partial_t\delta f+\theta v_\parallel\,\partial_y\delta f-\alpha\theta\,\partial_y\phi\,\partial_{v_\parallel}\delta f$$

$$=-\kappa\,\partial_y\phi\,f_0-\alpha\theta\,\partial_y\phi(v_\parallel/v_t^2)f_0\,, \tag{17}$$

where $\alpha=(1,-m_i/m_e)$ for the ions and the electrons, respectively; and we use the dimensionless gyrokinetic units of $y/\rho_s\to y$, $\Omega_i t\to t$, $v_\parallel/c_s\to v_\parallel$, and $e\phi/T_e\to\phi$. For this problem, we use $\kappa\equiv-\partial_x\ln n_0$ and have assumed a Maxwellian equilibrium. The gyrokinetic Poisson equation or the "quasineutrality" condition in one dimension is

$$\partial_{yy}\phi+\delta n_i=\delta n_e\,. \tag{18}$$

We solve these equations with a one-dimensional gyrokinetic simulation using the new method explained in Sec. II. In addition, a quiet-start technique employing Fibonacci numbers[3] has been used. In order to further minimize the noise, we have also used a cutoff scheme[6] of

$$w_i=\phi(x_i) \tag{19}$$

for the fast particles with $v_{\parallel\,i}\gg\omega/k_\parallel$. Here, ϕ_n is initially perturbed, where the n's are the Fourier harmonics of interest. Since our purpose is to study the nonlinear electron dynamics, we have also linearized the ion motion in the simulation by discarding the $\partial_{v_\parallel}\delta f$ term in Eq. (17), which is accomplished in the simulation by letting $v_\parallel=0$ for Eq. (4) and dropping the $(1-w_i)$ correction in Eq. (12).

The first run shown has the following parameters in the gyrokinetic units: $T_e/T_i=1$, $m_i/m_e=1837$, the magnetic field tilt is $\theta=0.01$, the particle size is 1 $(=\rho_s)$, the time step is $\Delta t=1$, $\kappa=0.2$, the system size is $L=16\Delta x$, the grid size is $\Delta x=0.5$, and the total number of particles is $N_{\text{tot}}=f_{16}=987$, where f_{16} denotes the sixteenth Fibonacci number. For the particles with $v_\parallel\geqslant 1.8v_{te}$, Eq. (19) is used

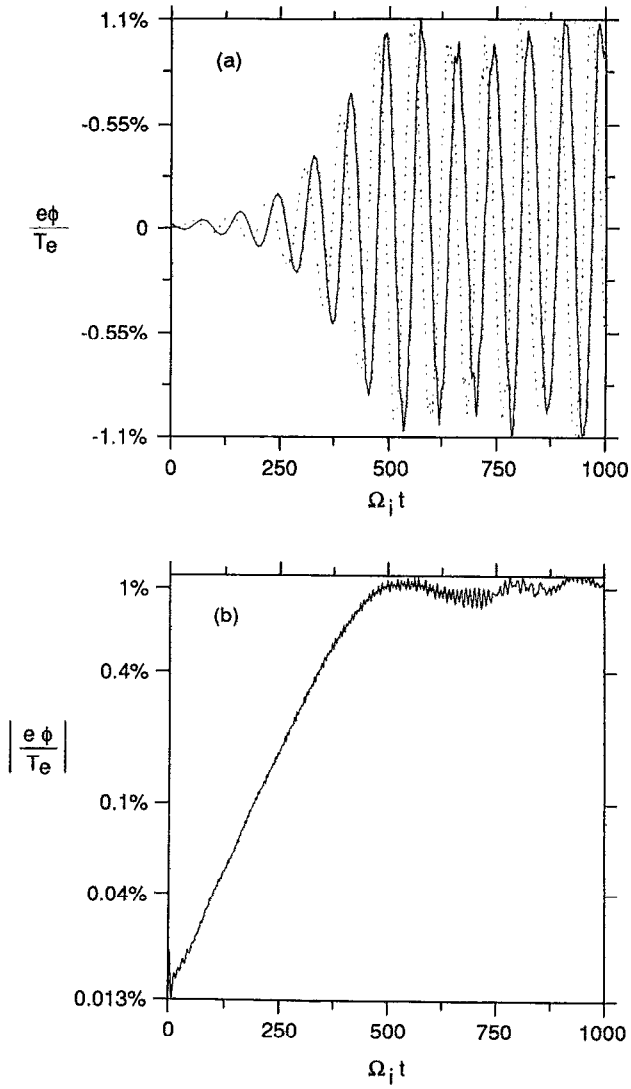

FIG. 1. The $n=1$ drift instability ($k_\perp \rho_i \simeq 0.8$) for the run with 987 particles on a 16-grid system. (a) The time history for the real (solid line) and imaginary (dashed line) parts of the electrostatic potential and (b) the corresponding amplitude evolution.

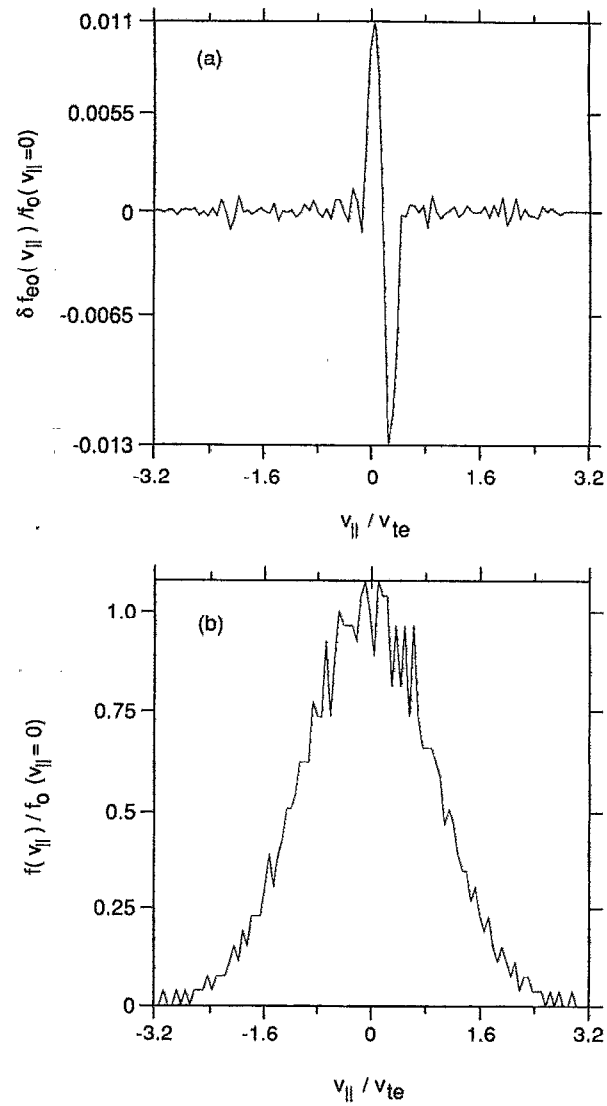

FIG. 2. The 987 particle run at $\Omega_i t = 500$. (a) The perturbed electron distribution $\delta f(k=0)/f_0(v_\parallel=0)$ and (b) the total electron distribution $f/f_0(v_\parallel=0)$.

for their weights. With this choice of parameters the dominant unstable mode is the $n=1$ harmonic or $k=2\pi/L \simeq 0.8$ mode.

Figure 1(a) shows the time evolution of the electrostatic potential for the $n=1$ Fourier mode. The real part is the solid line and the imaginary part is the dashed line. The mode frequency averaged over both the linear and nonlinear parts of the evolution is $\omega \simeq 0.075$. Figure 1(b) gives the logarithmic change of the amplitude as a function of time for this mode. A clean linear growth followed by a sudden nonlinear saturation is clearly visible. The measured linear growth rate is $\gamma \simeq 0.012$, and the saturation amplitude is $\phi \simeq 1.1\%$. Figure 2(a) shows the spatially averaged perturbation $\delta f_{e0} (\equiv \langle \delta f \rangle)$ at $t=500$ and gives the resonant point at $v_\parallel = 0.2 v_{te}$.

Integrating δf_{e0} in $v_\parallel$, we obtain $|\Sigma_i w_i / N_{\text{tot}}| \simeq 1.3 \times 10^{-4}$ at saturation ($t=500$) with a factor of 2.5 increase at the end of the run; thus the particle conservation deviates from Eq. (13). This discrepancy at the linear stage of the evolution can be understood from the fact that the one-dimensional continuity equation, obtained from Eq. (17), does not contain the usual particle flux term in x. To verify this point, we have carried out the simulation using the one-dimensional equation of Rath and Kaw,[12] which can be obtained from Eq. (17) by replacing f_0 with total f for the term associated with κ. In the linear stage of that simulation, the particle conservation is near perfect and the inaccuracy occurs only in the nonlinear stage due to numerical noise. Since the problem associated with particle nonconservation is minor and Eq. (17) is closely related to the more general equation, Eq. (1), we prefer not to carry on further with the Rath–Kaw equation.

Another interesting aspect of the simulation is that, while we are solving Eq. (17), we also follow the evolution

of the equation $\dot{f}=0$ with the same set of equations of motion and

$$f(y,v_{\parallel},t)=\sum_{i=1}^{N} S(y-y_i)\delta(v_{\parallel}-v_{\parallel i}). \tag{20}$$

The total distribution function f at $t=500$ is shown in Fig. 2(b). Its jaggedness, compounded by the fact that δf_{e0} is not at all discernible, would make it impossible to use this information for conservation property diagnostics, let alone for the field solve.

Because of the use of the linear ion response, the momentum conservation given by Eq. (15) cannot be satisfied in the simulation. However, we can use Eq. (14) to check a similar property. In the one-dimensional system, it becomes[13]

$$\frac{d}{dt}\left\langle \int v_{\parallel}\,\delta f_e\,dv_{\parallel}\right\rangle+\frac{m_i}{m_e}\theta\langle\Gamma_e\rangle=0, \tag{21}$$

where $\Gamma_e\equiv-\partial_y\phi\, n_e$ is the particle flux, and $\langle\cdots\rangle$ denotes spatial average. Hence we obtain a relationship between the rate of change of the momentum and the particle flux in the simulation, which is plotted in Fig. 3(a). Here, a frequency filter has been used to smooth the data for dp_e/dt and the normalization constant n_0 is the average number density. Apparently, numerical noise for the flux is quite substantial and there is a discrepancy of $O(10^{-4})$ between these two quantities. From Eq. (16), the energy conservation becomes

$$\left\langle \int \delta f v_{\parallel}^2\,dv_{\parallel}\right\rangle\Big/ n_0 v_t e^2+\langle|\partial_y\phi|^2\rangle=0. \tag{22}$$

This is shown in Fig. 3(b). Again, the results are quite noisy and the difference between the kinetic energy and the field energy is also of $O(10^{-4})$. However, considering the small number of particles used in the simulation, these results are actually quite good. We remind the reader that this was accomplished through the use of (1) the nonlinear characteristic method, (2) the quiet start technique, and (3) the nonrandom initial perturbation.

Nevertheless, the errors for the conservation properties after nonlinear saturation is somewhat troublesome, since our ultimate goal is to use the scheme to study long-time steady-state phenomena. To improve upon these results, we have carried out a series of runs and found that a substantial increase in numerical accuracy is needed. To illustrate this point, we now present a run with $\Delta t=0.2$, $N_{\text{tot}}=46\,368$ particles on a 64-grid system ($\Delta x=1/8$) using a particle size of $\rho_s/2$. All the other parameters remain the same. Figures 4(a) and 4(b) show the mode history. Comparing with the previous case, the mode frequency (averaged over both the linear and nonlinear parts of the evolution) increases slightly to $\omega\simeq0.088$, and the saturation level decreases slightly to $\phi\simeq1\%$, while the growth rate remains the same at $\gamma\simeq0.012$. One important difference is that the numerical (including noise) errors remain small in the nonlinear stage when the particles are trapped and executing bounce motion. This characteristic is clearly manifested in the diagnostics for the perturbed distribution

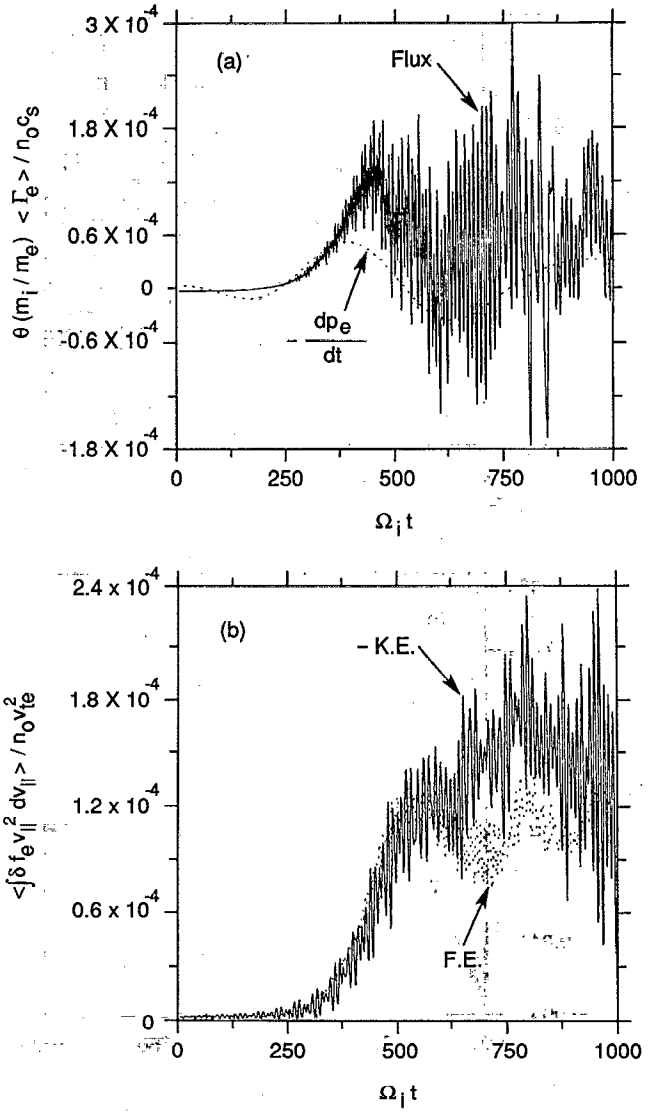

FIG. 3. The 987 particle run. (a) Time history for the electron particle flux (solid line) and the time rate of change for the electron parallel momentum (dashed line) and (b) the time evolution for the perturbed electron kinetic energy (solid line) and the field energy (dashed line).

function δf_{e0} and f in Figs. 5(a) and 5(b). However, for the perturbed distribution, which is also measured at $t=500$, the asymmetry in the velocity space still remains, and the corresponding discrepancy for the total particle number, $|\Sigma_i w_i/N_{\text{tot}}|$, is about 1.35×10^{-4} at saturation, which is similar to the previous fewer particle run. The difference now is that this discrepancy does not deteriorate after saturation. The source of this discrepancy was discussed earlier. Nevertheless, the overall smoothness of the distributions in Figs. 5(a) and 5(b) come from the increase in numerical accuracy. Interestingly, even with this type of accuracy, the perturbation of δf_{e0} is still not quite discernible in the total f diagnostic Fig. 5(b). This is because the perturbation is only a factor of 2 above the thermal fluctuation level of $\phi=1/\sqrt{N_{\text{tot}}}k\simeq0.6\%$.[1] Thus,

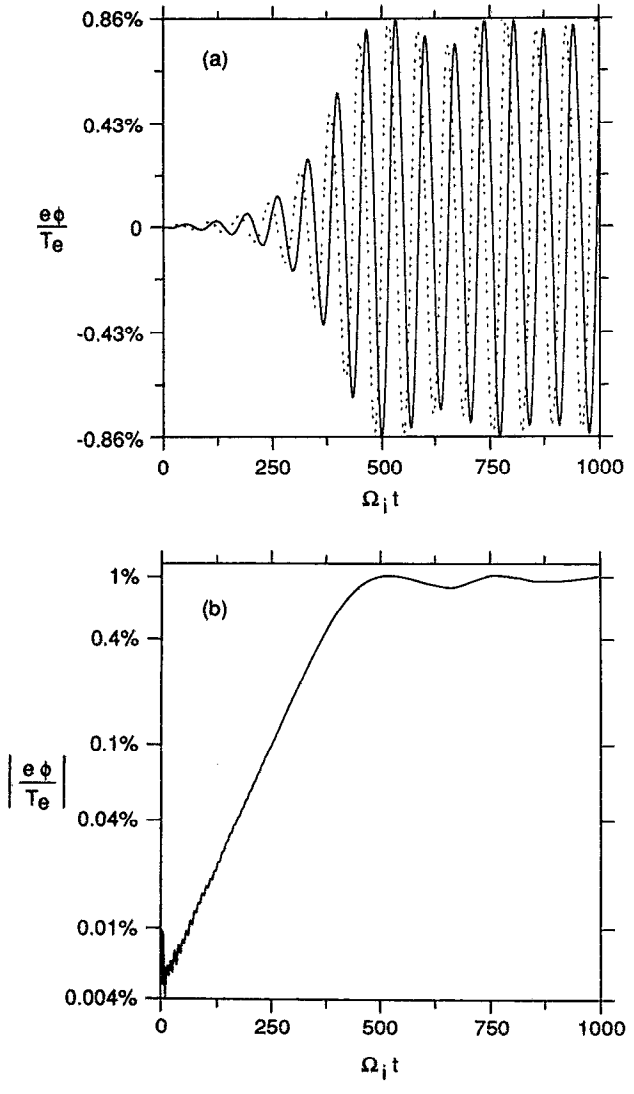

FIG. 4. The $n=1$ drift instability ($k_\perp \rho_i \simeq 0.8$) for the run with 46 368 particles on a 64-grid system. (a) The time history for the real (solid line) and imaginary (dashed line) parts of the electrostatic potential and (b) the corresponding amplitude evolution.

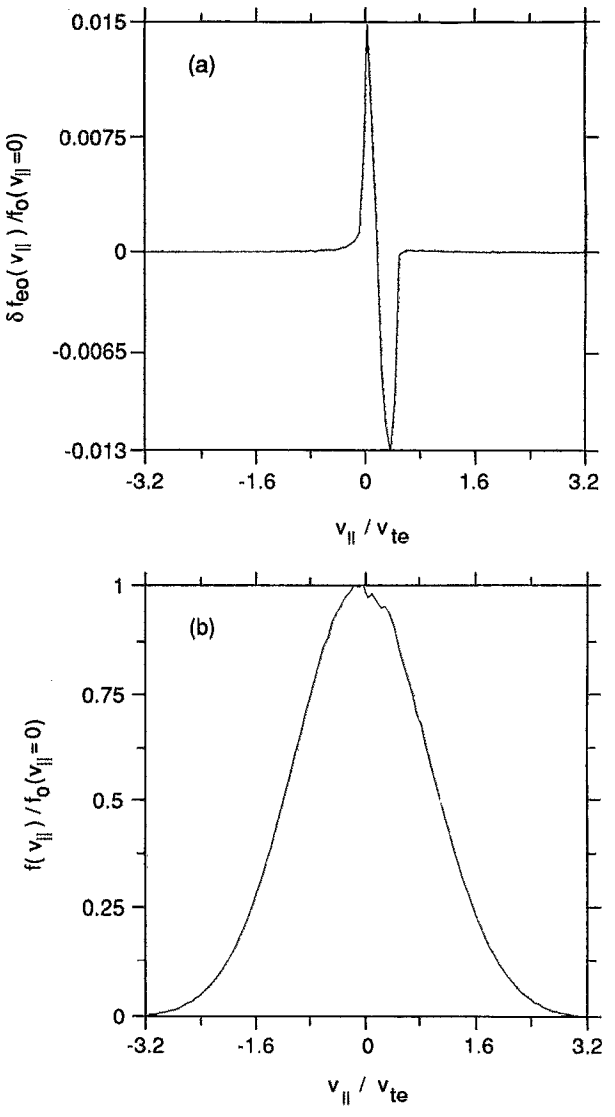

FIG. 5. The 46 368 particle run at $\Omega_i t=500$. (a) The perturbed electron distribution $\delta f(k=0)/f_0(v_\parallel=0)$ and (b) the total electron distribution $f/f_0(v_\parallel=0)$.

following from Ref. 6, one can surmise that a total f simulation, even with this many particles, would not give as clean a result as the new scheme. This point cannot be further verified, however, because there is no available scheme to solve the equation of the form $\dot{f}=-\kappa\,\partial_y\phi\, f_0$. The corresponding flux and energy diagnostics for this case are shown in Figs. 6(a) and 6(b). As we can see, the conservation of both these quantities are near perfect. The implication here seems to be that one still has to use a very large number of particles with enough spatial and time resolution to obtain reasonable conservation properties. On the other hand, a conventional particle simulation would need even more. However, if one is only interested in linear growth and nonlinear saturation, the present scheme represents a substantial savings in computing resources.

IV. NONLINEAR SATURATION

The nonlinear saturation of the most unstable modes (e.g., $n=\pm 1$ in the simulation results presented above) is due to the parallel velocity nonlinearity and is not caused by $E\times B$ advection. It is commonly accepted that the $E\times B$ nonlinearity, which is absent in the simple one-dimensional model, is the dominant nonlinearity for the saturation of the drift waves in the (more realistic) higher-dimensional models. However, the parallel nonlinearity does play a role in the saturation as was shown in Ref. 10. The simulation results in Sec. III indicate that the saturation level is much lower then $e|\phi|/T_e \sim \frac{1}{4}(k_\perp \rho_s)^2$, as predicted by Sagdeev and Galeev.[9] Also, in a tokamak geometry, drift-type modes are elongated in the radial direction ($k_r \ll k_\theta$), at least in the linear phase, which should reduce the effect of the $E\times B$ on saturation.[14–16] In addition, the

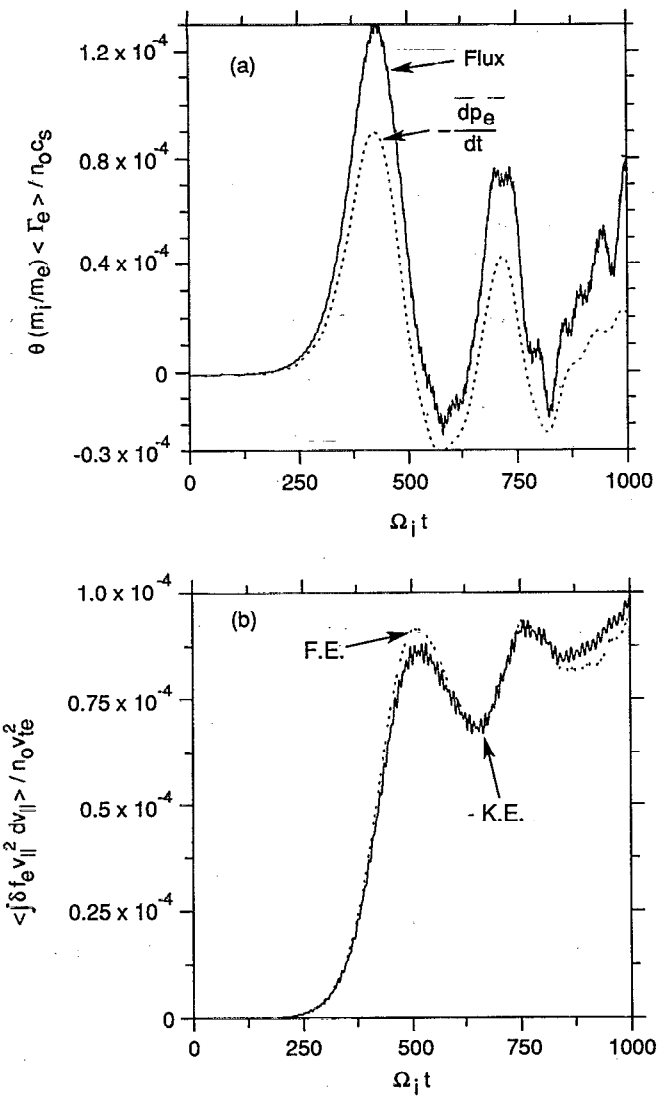

FIG. 6. The 46 368 particle run. (a) Time history for the electron particle flux (solid line) and the time rate of change for the electron parallel momentum (dashed line) and (b) the time evolution for the perturbed electron kinetic energy (solid line) and the field energy (dashed line).

parallel nonlinearity may be important in determining the steady-state transport caused by microturbulence.[11] The one-dimensional model allows us to isolate the parallel nonlinearity and study the associated physics.

In this section, we consider a simple case of three-wave coupling between the two fastest growing modes ($n=\pm 1$) and δf_0 for the electrons. The saturation takes place when the electron distribution is steepened at the resonance point $k_\parallel v_\parallel = \omega$. The saturation amplitude of the potential due to the $E_\parallel \partial_{v_\parallel} \delta f$ nonlinearity is calculated using a quasilinear estimate that is similar to the calculation for saturation of drift waves due to the $E\times B$ nonlinearity given in Ref. 10. In the following, we use the subscript "1" to label the fastest growing mode and its complex conjugate with $k=2\pi n/L$, where L is the system length, and n is the Fourier mode number. [Note that $\delta f_1(k) = \delta f_1^*(-k)$.] The governing drift-kinetic electron equations are

$$\partial_t \delta f_1 + ik_\parallel v_\parallel \delta f_1 + i(\omega_* - k_\parallel v_\parallel)\phi_1 f_0 + i(m_i/m_e)k_\parallel \phi_1 \partial_{v_\parallel} \delta f_0 = 0, \tag{23}$$

$$\partial_t \delta f_0 - 2(m_i/m_e)k_\parallel \phi_1 \partial_{v_\parallel} \mathrm{Im}(\phi_1 \delta f_1^*) = 0, \tag{24}$$

where $\omega_* = \kappa k$ (in the gyrokinetic units), f_0 is the background Maxwellian, and δf_0 is the nonlinear change of the background due to mode coupling. The perturbed electron density is $\delta n_{e1} = \int \delta f_1\, dv_\parallel$. For the ions, we assume a fluid response since $|\omega/k_\parallel| \gg v_{ti}$, and the continuity equation for ion density becomes

$$\partial_t \delta n_{i1} + i\omega_* \delta n_{i1} = 0. \tag{25}$$

Equations (18) and (23)–(25) could be solved using the Vlasov (Eulerian) simulation and should give the same results as the particle simulation in the previous section. However, to obtain an analytic estimate, we assume the dependence of $e^{-i\omega t}$ for δf_1, n_{i1}, and ϕ_1, where $\omega = \omega_r + i\gamma$ and also $|\omega_r/\gamma| \gg 1$. The perturbation can then be expressed as

$$\delta f_1 = \left(f_0 - \frac{(\omega_* - \omega_r)}{(k_\parallel v_\parallel - \omega)} f_0 - \frac{m_i}{m_e} \frac{k_\parallel}{(k_\parallel v_\parallel - \omega)} \partial_{v_\parallel} \delta f_0 \right) \phi_1 . \tag{26}$$

Assuming γ small, we can use the following relation

$$\frac{1}{(k_\parallel v_\parallel - \omega)} = \frac{k_\parallel v_\parallel - \omega_r + i\gamma}{|k_\parallel v_\parallel - \omega|^2} \simeq i\pi \delta(k_\parallel v_\parallel - \omega_r) \tag{27}$$

to obtain the electron density response as

$$\delta n_{e1} = \int_{-\infty}^{+\infty} \delta f_1\, dv_\parallel = \left(1 - i\sqrt{\frac{\pi}{2}} \frac{1}{k_\parallel v_{te}} (\omega_* - \omega_r) - \frac{m_i}{m_e} \int_{-\infty}^{+\infty} \frac{k_\parallel}{(k_\parallel v_\parallel - \omega)} \partial_{v_\parallel} \delta f_0\, dv_\parallel \right) \phi_1 , \tag{28}$$

from which we arrive at the following nonlinear dispersion relation:

$$1 + k^2 - \frac{\omega_*}{\omega} - i\sqrt{\frac{\pi}{2}} \frac{1}{k_\parallel v_{te}} (\omega_* - \omega_r) - \frac{m_i}{m_e} \int_{-\infty}^{+\infty} \frac{k_\parallel}{(k_\parallel v_\parallel - \omega)} \partial_{v_\parallel} \delta f_0\, dv_\parallel = 0. \tag{29}$$

Neglecting the nonlinear term (last term on the right), we obtain the familiar linear results[10]

$$\omega_r = \omega_l \equiv \omega_*/(1+k^2), \tag{30}$$

$$\gamma = \gamma_l \equiv \sqrt{\frac{\pi}{2}} \frac{1}{(k_\parallel v_{te})} \frac{\omega_l}{(1+k^2)} (\omega_* - \omega_l). \tag{31}$$

The predicted linear frequency and growth rate for the simulation are $\omega_l=0.0976$ and $\gamma_l=0.0134$, which are very close to the results shown in Figs. 1 and 4. From the linear response for δf_1, the nonlinear response of the background can be estimated as

$$\delta f_0=\pi(m_i/m_e)(k_\parallel/\gamma)|\phi_1|^2(\omega_*-\omega_l)\partial_{v_\parallel}[\delta(k_\parallel v_\parallel -\omega_l)f_0(v_\parallel)]. \tag{32}$$

Substituting Eq. (32) into Eq. (29), we obtain the nonlinear dispersion relation in terms of the amplitude of ϕ_1:

$$1+k^2-\frac{\omega_*}{\omega}-i\sqrt{\frac{\pi}{2}}\frac{1}{k_\parallel v_{te}}(\omega_*-\omega_l)\left[1-2\frac{k_\parallel^4}{\gamma_l^4}\left(\frac{m_i}{m_e}\right)^2|\phi_1|^2\right]=0. \tag{33}$$

From this equation, again assuming $|\gamma/\omega|\ll 1$, we obtain the same real frequency $\omega_r=\omega_l$, but the quasilinear value for the growth rate becomes

$$\gamma=\gamma_l\{1-2[(k_\parallel v_{te})^4/\gamma_l^4]|\phi_1|^2\}. \tag{34}$$

At saturation $\gamma=0$, the saturation level of the potential can be expressed as

$$|\phi_1|=\frac{1}{\sqrt{2}}\frac{\gamma_l^2}{(k_\parallel v_{te})^2}. \tag{35}$$

Using the simulation parameters of $k_\parallel=\theta 2\pi/L=0.007\,85$, $m_i/m_e=1837$, and $\gamma_l=0.0134$, the predicted saturation amplitude is $|\phi_1|=0.11\%$, which is an order of magnitude smaller than the level obtained from the simulation results shown in Figs. 1 and 4. Thus the effect of parallel nonlinearity on the saturation is overly estimated by the above approximation.

Next, to improve on this first estimate, we use the original form of the resonant denominator, Eq. (27), and also use the full nonlinear δf_1 to calculate δf_0, i.e.,

$$\delta f_0=\frac{m_i}{m_e}k_\parallel|\phi_1|^2(\omega_*-\omega_r)\partial_{v_\parallel}\left[\frac{f_0}{|k_\parallel v_\parallel-\omega_r|^2}\times\left(1+\frac{m_i}{m_e}\frac{k_\parallel}{(\omega_*-\omega_l)}\frac{\partial_{v_\parallel}\delta f_0}{f_0}\right)\right]. \tag{36}$$

If the quasilinear approximation is valid, this second-order ordinary differential equation could be solved to obtain δf_0, which, in turn, could be used in Eq. (29) to obtain an accurate prediction of the saturation level. The extra term included in Eq. (36) accounts for the effect of parallel trapping on saturation. To obtain a simpler estimate, we begin by using the δ-function relation, Eq. (27), in Eq. (36) to obtain

$$\delta f_0=(1-\alpha)f_0|_{v_\parallel=\omega_r/k_\parallel}(m_i/m_e)k_\parallel|\phi_1|^2\times(\omega_*-\omega_l)\partial_{v_\parallel}|k_\parallel v_\parallel-\omega|^{-2}, \tag{37}$$

where

$$\alpha=-\frac{m_i}{m_e}\frac{k_\parallel}{\omega_*-\omega_l}\frac{\partial_{v_\parallel}\delta f_0}{f_0}\Big|_{v_\parallel=\omega_r/k_\parallel}.$$

Then, substituting Eq. (37) in Eq. (29), assuming $|\omega/k_\parallel|\ll v_{te}$, and integrating, we obtain the following relation for the saturation amplitude:

$$|\phi_1|=(2/\sqrt{1-\alpha})\gamma_l^2/(k_\parallel v_{te})^2. \tag{38}$$

Assuming a linear response for δf_1, as was done in deriving Eq. (35), so that $\alpha=0$, we obtain $|\phi_1|=0.32\%$, which is in better agreement with the simulation results than Eq. (35), but it is still too low.

An estimate of α can be made by taking the derivative of Eq. (36) with respect to $v_\parallel$, and evaluate at $v_\parallel=\omega_r/k_\parallel$ to obtain

$$\partial_{v_\parallel}\delta f_0|_{v_\parallel=\omega_r/k_\parallel}=\frac{m_i}{m_e}k_\parallel|\phi_1|^2\Big\{(\omega_*-\omega_l)f_0(v_\parallel)\partial_{v_\parallel}^2|k_\parallel v_\parallel-\omega_r|^{-2}+\frac{m_i}{m_e}k_\parallel[(\partial_{v_\parallel}\delta f_0)\partial_{v_\parallel}^2+(\partial_{v_\parallel}^3\delta f_0)]\times|k_\parallel v_\parallel-\omega_r|^{-2}\Big\}_{v_\parallel=\omega_r/k_\parallel}, \tag{39}$$

where we have neglected derivatives of $f_0(v_\parallel)$ because it is slowly varying compared to $|k_\parallel v_\parallel-\omega_r|^{-2}$. We have also neglected $\partial_{v_\parallel}^2\delta f_0$ terms, by assuming δf_0 has the following form:

$$\delta f_0=C(t)v_\parallel\exp\left(-\frac{1}{2}\frac{u^2}{\Delta v_\parallel^2(t)}\right), \tag{40}$$

where $u=(v_\parallel-\omega/k_\parallel)$, C and $\Delta v_\parallel$ are independent of $v_\parallel$, and $\Delta v_\parallel\approx\sqrt{2|\phi_1(t)|(m_i/m_e)}$ is the width of the trapping region [see Fig. 5(a)]. From Eq. (40), one can show that $\partial_{v_\parallel}^2\delta f_0|_{v_\parallel=\omega_r/k_\parallel}=0$. In addition, we can use the relationship of $\partial_{v_\parallel}^3\delta f_0=-(3/\Delta v_\parallel^2)\partial_{v_\parallel}\delta f_0$, to obtain an equation for α, i.e.,

$$\alpha=2z^2/(2z^2+\tfrac{3}{2}z+1), \tag{41}$$

where $z=(v_{te}k_\parallel)^2/\gamma_l|\phi_1|$. We can now substitute this approximate value of α into Eq. (38) to obtain the following cubic equation:

$$\tfrac{3}{8}z^3-\tfrac{7}{4}z^2-\tfrac{3}{2}z-1=0. \tag{42}$$

Solving Eq. (42), we find

$$|\phi_1|=5.48[\gamma_l^2/(k_\parallel v_{te})^2] \tag{43}$$

along with two spurious complex roots with negative real parts. Equation (43) yields $|\phi_1|=0.87\%$ for our simulation parameters, which is in good agreement with the results shown in Figs. 1 and 4. We have also tried an iterative solution using the linear value of δf_1 to obtain the first iteration $\delta f_0^{(1)}$, then using $\partial_{v_\parallel}\delta f_0^{(1)}$ in Eq. (36) to predict $\delta f_0^{(2)}$, etc. However, this procedure did not converge.

V. GENERAL NONLINEAR CHARACTERISTIC METHOD

In this section, we extend the nonlinear scheme previously discussed for the electrostatic slab in Sec. II to the general electromagnetic gyrokinetic equations. We begin, as before, by writing $f(\mathbf{z},t)=f_0(\mathbf{z})+\delta f(\mathbf{z},t)$, where $\mathbf{z}=(\mathbf{R},v_\parallel,\mu)$, and $f_0(\mathbf{z})$ is an equilibrium distribution that satisfies $\dot{\mathbf{z}}_0\cdot\partial_z f_0(\mathbf{z})=0$. Using the electromagnetic gyrokinetic equations with a nonuniform equilibrium B field[17–20] and writing $\dot{\mathbf{z}}$ as equilibrium and perturbed parts, $\dot{\mathbf{z}}=\dot{\mathbf{z}}_0+\dot{\mathbf{z}}_1$, the equation for δf is

$$\partial_t(B^*\delta f)+\partial_z\cdot(\dot{\mathbf{z}}B^*\delta f)=-\dot{\mathbf{z}}^1\cdot\partial_z f_0, \tag{44}$$

where $\mu\equiv mv_\perp^2/(2B)$ is time independent, and the equilibrium and perturbed trajectories are evolved using

$$\dot{\mathbf{R}}^0=\frac{1}{B^*}\left[v_\parallel\,\mathbf{B}^{*0}+(c/e)\hat{\mathbf{b}}\times\mu\nabla B^0\right], \tag{45}$$

$$\dot{v}_\parallel^0=-\frac{1}{B^*}\left[\mathbf{B}^{*0}\cdot(\mu/m)\nabla B^0\right], \tag{46}$$

$$\dot{\mathbf{R}}^1=\frac{1}{B^*}\left[v_\parallel\,\delta\mathbf{B}_\perp+(c/e)\hat{\mathbf{b}}\times\mu\nabla\delta B_\parallel+c\hat{\mathbf{b}}\times\nabla\delta\phi\right], \tag{47}$$

$$\dot{v}_\parallel^1=-\frac{1}{B^*}\left[\mathbf{B}^{*0}\cdot\left(\frac{\mu}{m}\nabla\delta B_\parallel+\frac{e}{m}\nabla\delta\phi+\frac{e}{mc}\partial_t\delta A_\parallel\,\hat{\mathbf{b}}\right)+\delta\mathbf{B}_\perp\cdot\frac{\mu}{m}\nabla B^0\right], \tag{48}$$

where $\hat{b}=\mathbf{B}^0/B^0$, $\mathbf{B}^*=\mathbf{B}^0+\delta\mathbf{B}_\perp+(mc/e)v_\parallel\nabla\times\hat{\mathbf{b}}$, $B^*=\hat{\mathbf{b}}\cdot\mathbf{B}^*$, $\mathbf{B}^{*0}=\mathbf{B}^0+(mc/e)v_\parallel\nabla\times\hat{\mathbf{b}}$, and $\mathbf{B}^0$ is the equilibrium magnetic field.

The characteristics (or particles) follow the full nonlinear trajectories $\mathbf{z}=\mathbf{z}^0+\mathbf{z}^1$, and δf is represented by

$$B^*\delta f(\mathbf{z},t)=\sum_i w_i\delta(\mathbf{z}-\mathbf{z}_i). \tag{49}$$

We define g as a smooth distribution function representing the particle distribution (g does not necessarily have to be equal to the physical distribution function f at this point), and assume

$$B^*g(\mathbf{z},t)=\sum_i\delta(\mathbf{z}-\mathbf{z}_i). \tag{50}$$

Substituting Eq. (49) into Eq. (44) and using Eq. (50), we obtain

$$\dot{w}_i=-\left(\dot{\mathbf{z}}^1\cdot\frac{\partial_z f_0}{g(\mathbf{z},t)}\right)_{\mathbf{z}=\mathbf{z}_i,t}=-\dot{\mathbf{z}}^1\cdot\frac{\partial_z f_0(\mathbf{z}_i)}{g(\mathbf{z}_i,t=0)}, \tag{51}$$

which is just the generalization of Eq. (11). If, as before, we take $g=f=f_0+\delta f$, we obtain

$$\dot{w}_i=-(1-w_i)\left(\dot{\mathbf{z}}^1\cdot\frac{\partial_z f_0}{f_0}\right)_{\mathbf{z}=\mathbf{z}_i,t}. \tag{52}$$

This evolution equation for w_i along with the equations for the nonlinear trajectories equations (45)–(48), is the more general version of the new method presented in Sec. II.

VI. DISCUSSION

We have developed a new nonlinear characteristic method that retains all nonlinearities in a consistent way. This, however, does not preclude the possibility of neglecting various nonlinear terms if they are physically unimportant. In fact, various terms can easily be "turned on and off" to test their physical effect. We also see no immediate difficulties in applying this method to other Vlasov–Maxwell systems where the derivatives of the initial distribution are known and finite. For a strong instability, where the perturbations become large $\delta f/f\approx 1$, noise properties revert back to those of a conventional particle simulation. However, in such a case, the linear phase would be much more accurately resolved. At best, the new method captures the physics of conventional particle schemes with improved statistical properties. At worst, the scheme behaves linearly (with very low noise properties) for small perturbations, and fully nonlinear (with associated thermal noise) for large perturbations, and consistently makes the transition between the two extremes. We were able to obtain good energy conservation. However, compared to the number needed to capture the relevant physics of the drift wave model, a very large number of particles was required. The saturated electrostatic energy and associated change in electron kinetic energy is only 0.01% of the total electron thermal energy for the choice of parameters in Sec. III. As such, it is not surprising that a relatively large number of particles, small time step and fine grid were required to resolve this small change in kinetic energy (0.01% of the total).

This one-dimensional drift wave model permits us to isolate $E_\parallel\,\partial_{v_\parallel}\delta f$ nonlinearity and the associated nonlinear physics. Mode coupling theory was used to obtain a saturation level that is much lower (for our choice of parameters) than the estimate based on the energy balance calculation of Sagdeev and Galeev.[9] Simulation results agree well with our estimate. Because of this new lower saturation amplitude, parallel velocity nonlinearity may play a more important role in microturbulence then previously thought, although past investigations have shown such a tendency.[10] In addition, the existing linear theory for tokamak geometry predicts a ballooning-type mode structure which is elongated in the radial direction,[14–16] and therefore will reduce the effectiveness of the $E\times B$ nonlinearity for saturation.

Finally, the nonlinear characteristic method was extended to the general electromagnetic gyrokinetic equations. Application of these equations in a three-dimensional toroidal simulation is an ongoing effort and will be reported in the future.

ACKNOWLEDGMENTS

We thank Liu Chen, T. S. Hahm, A. M. Dimits, S. Rath, and J. Denavit for enlightening discussions.

This research was supported, in part, by an appointment to the U.S. Department of Energy Fusion Energy Postdoctoral Research Program administered by Oak Ridge Associated Universities and by DOE Contract No. DE-AC02-76-CHO-3073.

[1]W. W. Lee, J. Comput. Phys. **72**, 243 (1987).
[2]J. A. Byers (private communication, 1970).
[3]J. Denavit and J. M. Walsh, Comments Plasma Phys. Controlled Fusion **6**, 209 (1981).
[4]B. I. Cohen, S. P. Auerbach, J. A. Byers, and H. Weitzner, Phys. Fluids **23**, 2529 (1980).
[5]A. Friedman, R. N. Sudan, and J. Denavit, J. Comput. Phys. **40**, 1 (1980).
[6]A. M. Dimits and W. W. Lee, "Partially linearized algorithms in gyrokinetic particle simulation," to appear in J. Comput. Phys.
[7]T. Tajima and F. W. Perkins (private communication, 1983).
[8]M. Kotschenruether, Bull. Am. Phys. Soc. **34**, 2107 (1988).
[9]R. Z. Sagdeev and A. A. Galeev, *Nonlinear Plasma Theory* (Benjamin, New York, 1969).
[10]W. W. Lee, J. A. Krommes, C. R. Oberman, and R. A. Smith, Phys. Fluids **27**, 2652 (1984).
[11]W. W. Lee and W. M. Tang, Phys. Fluids **31**, 612 (1988).
[12]S. Rath and P. K. Kaw, "Nonlinear drift phase-space structures," to appear in J. Plasma Phys.
[13]W. M. Nevins, Phys. Fluids **22**, 1681 (1979).
[14]S. C. Cowley, R. M. Kulsrud, and R. Sudan, Phys. Fluids B **3**, 2767 (1991).
[15]F. Romanelli, L. Chen, and S. Briguglio, Phys. Fluids B **3**, 2496 (1991).
[16]S. E. Parker and W. W. Lee, Bull. Am. Phys. Soc. **36**, 2280 (1991).
[17]T. S. Hahm, W. W. Lee, and A. J. Brizard, Phys. Fluids **31**, 1940 (1988).
[18]T. S. Hahm, Phys. Fluids **31**, 2670 (1988).
[19]A. J. Brizard, J. Plasma Phys. **41**, 541 (1989).
[20]A. J. Brizard, Ph.D. thesis, Princeton University, 1990.